machines

MDPI

Article

Forced Response Assessment of Cracked Aerospace Structures Using VIBRANT

Mertol Tüfekci [1,2]

[1] Centre for Engineering Research, University of Hertfordshire, Hatfield AL10 9AB, UK; m.tufekci@herts.ac.uk
[2] School of Physics, Engineering and Computer Science, University of Hertfordshire, Hatfield AL10 9AB, UK

Abstract

This study presents an assessment of forced vibration responses of cracked beam-type aerospace structures using VIbration BehaviouR ANalysis Tool (VIBRANT), a high-fidelity time-marching analysis platform. The methodology captures contact-induced nonlinearities arising when crack surfaces intermittently open and close during vibration, producing time-varying stiffness and damping. Frequency-domain behaviour is extracted from time-domain simulations of beams representing aero-engine blades and wing structures under various crack configurations. Results reveal that a crack-induced nonlinearity is strongly configuration-dependent: only specific combinations of crack depth, position relative to the moment distribution, and excitation amplitude produce detectable nonlinear signatures, whilst other configurations—including cracks representing significant structural compromise—exhibit quasi-linear response that would evade conventional vibration-based detection. The deeper crack configuration activates breathing behaviour at higher forcing levels, leading to rightward resonance frequency shifts and amplitude reductions due to impact and frictional contact damping, whereas the baseline and repositioned crack configurations maintain a quasi-linear response across all forcing levels examined. This configuration-dependent character of the breathing crack nonlinearity—and in particular the conditions under which nonlinear signatures are absent despite active damage—represents a critical finding for structural health monitoring and maintenance planning in aerospace applications.

Keywords: nonlinear system modelling; nonlinear dynamics; time-marching; forced response; aerospace structures

Academic Editors: Farshid Torabi, Kamran Foroutan and Tamara Nestorović

Received: 30 December 2025
Revised: 25 March 2026
Accepted: 27 March 2026
Published: 29 March 2026

1. Introduction

Modern engineering structures such as aero-engine components and wind turbine blades are subject to complex dynamic loads that often induce significant deformations and nonlinear behaviour. In particular, bladed disc assemblies in aircraft engines operate under extreme conditions where large deflections, contact interactions and nonlinear material properties critically influence their forced vibration response [1–8]. To ensure structural integrity and reliable performance, engineers have developed various modelling techniques. Frequency-domain approaches—most notably the Harmonic Balance Method (HBM)—approximate the nonlinear equations by decomposing the response into a series of harmonics, thus converting time-dependent problems into a set of algebraic equations [9–11]. The HBM is particularly effective for periodic solutions in large-scale systems and has been utilised for applications ranging from unsteady nonlinear

behaviour [10] to stochastic analyses under uncertainty [12] and model order reduction for intricate geometries [13]. In contrast, time-marching methods solve the full nonlinear differential equations directly in the time domain, capturing transient effects and the complete harmonic content at higher computational expense [14–17]. Despite this computational cost, these techniques have proven robust for capturing the intricate dynamics of systems such as frictional brake assemblies. Recent progress—including pseudotime stepping and multigrid acceleration—has further improved their computational efficiency, making them viable for complex engineering applications [10,18,19].

Research has led to the development of specialised techniques that blend frequency- and time-domain approaches. For example, HBM variants—such as the Receptance HBM and the Global Residue HBM—have been refined to efficiently handle frictional and contact-induced nonlinearities in rotating systems [20,21]. Moreover, hybrid approaches integrating finite element modelling with frequency-domain techniques have emerged to capture both the spatial and temporal aspects of dynamic behaviour [10,22–24].

The integration of the HBM with continuation methods allows researchers to track periodic solutions as system parameters vary, thereby capturing complex bifurcation scenarios and multi-valued Frequency Response Functions (FRFs) [18,25]. Recent advances in bifurcation tracking methodologies have extended these capabilities to systems with parameter-dependent excitations [26], the optimisation of nonlinear energy sinks under harmonic forcing [27], and robust design against vibro-impact phenomena [28]. This combined approach is particularly effective for systems such as turbine blade–disc assemblies with underplatform dampers, where it is crucial to accurately predict contact pressures and include zero-harmonic contributions in the multiharmonic expansion [22,23]. Additional techniques, such as quasi-linearisation, further simplify the analysis by transforming the nonlinear differential equations into algebraic forms [24].

Advanced computational tools have emerged to address these challenges. Software packages like NLvib are adept at simulating nonlinear structural behaviour, whilst specialised tools such as MANLAB and Mousai provide powerful capabilities for exploring nonlinear periodic solutions through continuation and harmonic balance solvers [29–31]. Proprietary codes, including FORSE from Imperial College London and PERMAS from Intes, offer additional capabilities for modelling forced responses in nonlinear systems [6,32–38]. These computational frameworks have been successfully applied to diverse engineering problems, including large-scale geared systems with vibro-impact responses [39], periodic waveguides with localised nonlinearities [40], and damage detection in structures with unknown local nonlinearities [41].

Mechanical systems with impact nonlinearities—often known as vibro-impact oscillators—exhibit a broad spectrum of dynamic behaviours that have drawn extensive attention over recent decades. In these systems, an oscillating mass intermittently collides with a barrier, thus introducing a non-smooth nonlinearity that markedly alters the FRF relative to a linear system [39]. The presence of impacts results in a piecewise variation in stiffness; for instance, when the mass strikes the barrier the effective stiffness rises abruptly, leading to a shift or splitting of the resonance peak, whereas a gap prior to impact introduces a softening effect at lower amplitudes. Nordmark's work [42] on grazing bifurcations illustrated that minor perturbations at the onset of contact could provoke a cascade of period-doubling bifurcations and chaos.

Comprehensive overviews by Ibrahim [43] and Babitsky [44] have detailed analytical strategies for tackling such systems, including piecewise analytical solutions and non-smooth coordinate transformations that address velocity discontinuities. Experimental validation has been provided by Ing et al. [45], who investigated an impact oscillator with a one-sided elastic constraint, thereby demonstrating the onset of chaotic behaviour

and multiple coexisting periodic responses. Rebouças [46] further compared modelling approaches—contrasting contact force models with restitution-based methods—to reconcile analytical, numerical, and experimental FRFs. The FRF of an impact oscillator is fundamentally distinct from that of a linear system, exhibiting amplitude-dependent stiffness, multiple coexisting attractors, abrupt transitions and rich harmonic content. Advanced numerical techniques combining the HBM with grazing bifurcation analysis have proven particularly effective for investigating vibro-impact phenomena in complex mechanical systems [28,39]. The most directly relevant studies, namely, those by Nordmark [42], Ibrahim [43], Babitsky [44], Ing et al. [45], Rebouças [46], Karkar et al. [18], Stefani et al. [25], Fang et al. [47], Liu and Khulief [48] and Bruns et al. [49], provide a robust theoretical and experimental foundation for understanding and modelling these non-smooth dynamics.

Within this broader context of nonlinear structural dynamics, breathing cracks represent a particularly important class of damage that introduces bilinear stiffness behaviour. Breathing cracks open and close during vibration cycles, creating time-varying stiffness that manifests as distinct nonlinear phenomena [50,51]. Recent studies have developed sophisticated modelling approaches for breathing cracks, including semi-analytical methods for rotating blades [52], modal analysis techniques accounting for internal resonance effects [53], and comprehensive frameworks for crack identification and localisation [54,55]. These investigations demonstrate that breathing crack behaviour is highly sensitive to crack parameters and operating conditions, making nonlinear vibration analysis a promising approach for structural health monitoring. It is well documented that, depending on excitation frequency and amplitude, breathing cracks may generate sub-harmonic and super-harmonic components due to partial closure and intermittent contact, particularly when impact-like interactions occur [56]. However, these nonlinear frequency components are strongly regime-dependent and may be absent when crack breathing remains smooth or weakly activated.

Early and well-established numerical studies have demonstrated that breathing cracks in beam-like structures can be effectively modelled through bilinear or unilateral stiffness formulations. Iterative time-domain approaches and reduced-order finite element models have been successfully employed to capture crack opening–closing behaviour and its influence on forced-response characteristics [57,58]. These studies show that crack breathing introduces time-varying stiffness governed by the interaction between excitation level, crack geometry, and local contact conditions, leading to amplitude-dependent dynamic behaviour even in geometrically simple beam configurations.

The engineering significance of studying crack-induced nonlinear dynamics in aerospace structures is multifold. First, breathing cracks introduce subtle amplitude-dependent behaviour that conventional linear modal analysis cannot detect, requiring advanced nonlinear techniques for reliable identification. Second, understanding the transition from quasi-linear to measurably nonlinear response as crack severity increases enables the development of damage thresholds for maintenance scheduling. Third, the effects of crack location and moment distribution on detectability are examined, providing knowledge that is critical for optimising sensor placement and inspection protocols in operational aircraft. Finally, accurate prediction of crack breathing effects under realistic forcing conditions supports risk assessment and remaining life estimation, directly contributing to flight safety and operational reliability.

Modern experimental validation increasingly relies on non-contact optical measurement techniques that complement computational approaches for lightweight aerospace structures. Digital Image Correlation (DIC) has emerged as a powerful full-field measurement method for modal analysis, offering significant advantages over traditional point-wise sensors such as accelerometers [59,60]. Recent advances in optical systems—including laser Doppler

vibrometry, stereo-photogrammetry, and phase-based motion magnification—have extended measurement capabilities to rotating structures, high-frequency modes, and micro-scale deformations [61,62]. Three-dimensional vibration measurements with optical systems employ enhanced methodologies such as multi-view configurations, telecentric lenses, and virtual speckle patterns to address challenging measurement scenarios [63,64]. These experimental techniques provide essential validation data for computational platforms and enable correlation between numerical predictions and physical behaviour, representing a complementary approach to advancing structural dynamics characterisation for aerospace applications.

Computational investigation of breathing crack dynamics has been extensively advanced through finite element implementations using commercial software. Andreaus and colleagues employed contact formulations in ADINA (Bentley Systems, https://www.bentley.com/software/adina/, accessed on 28 February 2026) to examine harmonically forced cracked beams, identifying sub- and super-harmonic responses characteristic of bilinear stiffness behaviour and demonstrating that nonlinear forced-response characteristics enable experimental damage detection [65–67]. Ma and co-workers developed specialised cracked beam elements validated against commercial finite element models for rotating blades, investigating crack breathing mechanisms under combined aerodynamic forcing and centrifugal effects whilst examining the influence of crack parameters on vibration characteristics and breathing status [68,69]. Independently, Al-Qaradawi et al. [70] examined nonlinear dynamic characteristics of a cracked blade using ANSYS (ANSYS, Inc., Canonsburg, PA, USA; https://www.ansys.com, accessed on 28 February 2026), further demonstrating the applicability of commercial finite element tools to breathing crack problems. These established finite element approaches have demonstrated that breathing cracks produce distinctive harmonic content, amplitude-dependent frequency shifts, and characteristic whirl orbits in rotating systems, providing foundations for vibration-based crack detection methodologies.

This study presents a high-fidelity numerical assessment of cracked beams as aerospace components under forced vibrations using VIBRANT: VIbration BehaviouR ANalysis Tool [8,19,71]. VIBRANT employs a time-marching approach to extract the frequency-domain behaviour of mechanical systems, enabling realistic predictions of vibrational response even when cracked surfaces come into contact during vibration, thereby introducing nonlinearity and altering structural stiffness. The methodology accurately captures both transient and steady-state dynamics despite the presence of various nonlinearities associated with damage. Time-domain simulations are performed on beam models representing aero-engine blades and wing structures with crack configurations, and the resulting data are transformed to determine the forced response across a range of operating conditions. The results reveal that crack-induced nonlinear behaviour is subtle and strongly configuration-dependent, with only specific combinations of crack depth, location, and forcing amplitude producing detectable nonlinear signatures, a finding with direct implications for the design of vibration-based damage detection strategies.

Whilst VIBRANT's general architecture and validation have been established in previous publications [8,19,71], the present work constitutes its first application to breathing crack problems, providing novel insights into the configuration-dependent nature of crack-induced nonlinear dynamics. The central contribution lies in the systematic parametric investigation revealing that detectable nonlinear signatures—specifically rightward frequency shifts and normalised amplitude reduction—emerge only under specific combinations of crack depth, position, and forcing level, whilst other crack configurations representing comparable structural compromise produce quasi-linear response that would be difficult to distinguish from undamaged behaviour using conventional

vibration-based monitoring. The demonstration that crack position relative to mode shape and moment distribution critically determines whether nonlinearity manifests—and thus whether damage is detectable—has direct implications for structural health monitoring protocols in aerospace applications.

Although the present work represents the first application of VIBRANT to breathing-crack dynamics, the validation philosophy follows established practice in nonlinear structural dynamics: numerical frameworks are commonly verified against accepted reference problems and benchmark trends before being extended to new nonlinear phenomena. In the specific context of breathing cracks, classical analytical and experimental studies have shown that opening–closing behaviour produces an effective bilinear stiffness and a reduced frequency drop relative to an always-open crack, with the dominant response depending on the interplay between preload and vibration amplitude [72]. More broadly, benchmark-driven validation is standard in nonlinear forced-response modelling of contact/friction and vibro-impact phenomena, where trend-level agreement in resonance shift, peak amplitude evolution, and harmonic content is often the primary indicator of physical consistency prior to application to more complex geometries and operating conditions [73,74]. Recent review studies further emphasise that breathing-crack-induced nonlinearity manifests through a wide range of mechanisms, including bilinear stiffness variation, amplitude-dependent damping, and harmonic generation, with the dominant features depending strongly on operating regime and modelling assumptions [54].

It is emphasised that the present study is positioned as a clear and reproducible set of reference cases, intended to illustrate the proposed modelling workflow and the capabilities of the VIBRANT framework for analysing crack-induced nonlinear dynamics. A simplified structural configuration is therefore adopted to allow the underlying nonlinear mechanisms to be examined in a transparent manner, without introducing additional sources of complexity. Whilst more detailed models incorporating additional physical effects and geometric features are essential for specific engineering applications, the chosen level of abstraction here serves to facilitate interpretation, reproducibility, and comparison, and to provide a baseline that can be readily extended in future studies.

2. Overview of VIBRANT's Architecture

VIBRANT: VIbration BehaviouR ANalysis Tool is a computational platform designed to facilitate time-marching frequency-sweep analyses for diverse mechanical systems. By integrating the simulation capabilities of Abaqus 2024 (Dassault Systèmes, Vélizy-Villacoublay, France; https://www.3ds.com/products/simulia/abaqus, accessed on 28 February 2026) with a robust Python 3.11 (Python Software Foundation, https://www.python.org, accessed on 28 February 2026) scripting environment, the platform automates complex workflows to achieve high reliability and accuracy in dynamic analyses. VIBRANT is engineered to address a large variety of nonlinear phenomena such as contact interactions, localised plasticity, large deformations, and energy dissipation induced by damping. In addition, the platform supports multiphysics simulations. To manage the computational demands associated with these analyses, parallel processing techniques are employed, making VIBRANT a useful tool for applications in aerospace and mechanical engineering [8,19,71].

2.1. Framework and Toolchain

The platform is built upon a suite of established software utilities that manage model configuration, simulation execution, and result visualisation. Abaqus is utilised as the primary finite element analysis software, while Python scripts coordinate automation and data-handling processes. Numerical computations are performed using

NumPy 1.26 (https://numpy.org, accessed on 28 February 2026), and **Matplotlib** 3.8 (https://matplotlib.org, accessed on 28 February 2026) is employed to generate visual representations of the results. Standard Python libraries, including `os`, `math`, and `time`, are also incorporated to support system-level operations, tracking and debugging.

For proper operation, it is necessary that both Python and Abaqus are correctly installed and configured. The accompanying scripts should either be located in the same directory as the Abaqus files or have their paths specified to ensure proper integration.

2.2. Process Flow

The VIBRANT workflow begins with the setup stage, where the frequency range, nodes, and amplitude values are defined and the necessary data structures are initialised. This is followed by the preparation step, during which the Abaqus models are updated for each specified frequency and the corresponding modifications are saved. In the execution phase, these updated models are submitted to Abaqus and the simulation progress is closely monitored. Once the simulations are completed, the processing step extracts the relevant data, computes the system responses, and stores the results for further analysis. The subsequent management phase involves organising the generated files and creating plots for visualisation, ensuring that all outputs are appropriately saved. Finally, in the finalisation stage, the results are compiled and summarised, including the reporting of computational time and resources used, thereby completing the workflow. Figure 1 shows the flowchart that outlines the sequential steps executed by the VIBRANT platform.

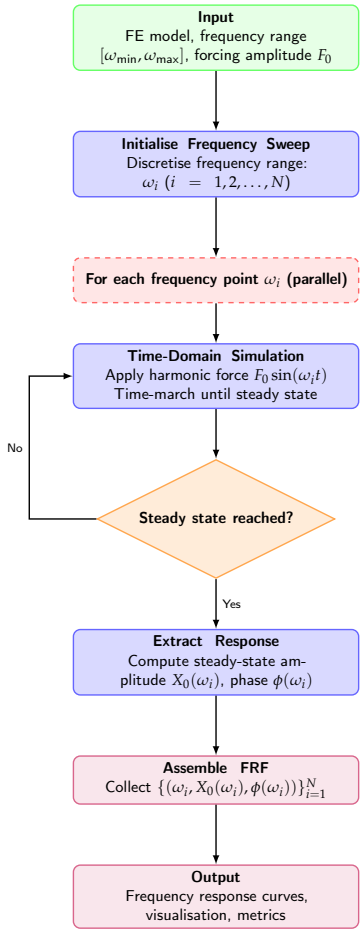

Figure 1. Computational process of the VIBRANT platform for frequency sweep analysis.

3. Representative Cracked Beam/Blade

3.1. Description of the System

A cantilever beam was adopted to represent a simplified cracked blade under vibrational loading. As shown in Figure 2, the beam is fixed at one end and subjected to a concentrated sinusoidal force at the free tip. A crack is introduced near the clamped region, reflecting the type of damage that often emerges towards the end of an aerospace component's operational life. The crack depth is denoted by b, while the intact (undamaged) cross section is indicated by b'. a denotes the distance between the crack and the free end and a' indicates the distance between the crack and the fixed boundary. For clarity, the beam has a total length of 800 mm, a width of 80 mm, and a thickness of 2 mm (perpendicular to the page).

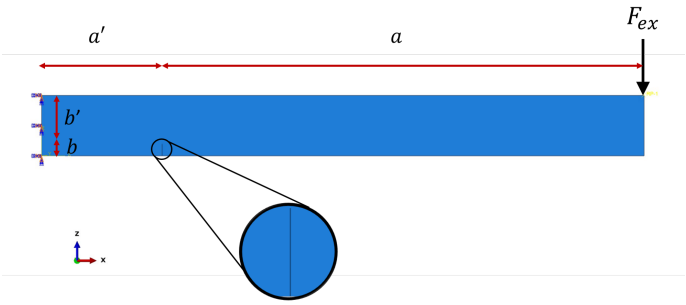

Figure 2. Schematic of the representative cracked beam model representing a blade. The beam is clamped on the left and excited by a sinusoidal force at the free tip.

The material was chosen as Ti–6Al–4V, with an elastic modulus of 110 GPa, a Poisson's ratio of 0.31, and a density of 4600 kg/m^3. This alloy is widely used in aerospace applications due to its high strength and stiffness-to-weight ratio and considerable fatigue resistance.

During vibration, the cracked surfaces may intermittently come into contact, introducing nonlinearity into the system's dynamic response and altering its effective stiffness. In the numerical model, the crack contact was defined as a hard contact in the normal direction and frictional in the tangential direction, with a friction coefficient of 0.1.

For the purposes of this study, the forced response was measured at the same free-tip node where the sinusoidal force is applied. This ensured a consistent reference for amplitude and phase, allowing direct observation of how crack-induced nonlinearity influenced the beam's response across a range of operating conditions. Consequently, this beam serves as a convenient test case for studying the impact of crack-induced nonlinearity on forced vibrations in structures representative of aero-engine blades and wing components.

3.2. Finite Element Model Description

The representative beam was modelled using a three-dimensional finite element formulation implemented in Abaqus/Standard. The structure was discretised using quadratic tetrahedral solid elements, which are suitable for capturing bending-dominated deformation and local stress gradients near geometric discontinuities. The final finite element mesh consisted of 4208 elements, with local refinement applied in the vicinity of the crack to accurately resolve contact interactions between the crack faces.

The crack was explicitly represented as a geometric notch, allowing the opposing crack surfaces to undergo intermittent opening and closure during vibration. Contact between the crack faces was enforced using a hard-contact formulation in the normal direction to prevent interpenetration, and a Coulomb friction model in the tangential direction with a friction coefficient of 0.1. This formulation enabled physically realistic represen-

tation of crack breathing behaviour and associated frictional energy dissipation without introducing artificial compliance through penalty stiffness.

The beam was fully clamped at the left end, with all translational and rotational degrees of freedom constrained. The excitation was applied at the free end as a sinusoidal surface traction, producing transverse bending deformation. The structural response was obtained through time-domain numerical integration, and steady-state vibration characteristics were extracted from the converged periodic response.

To assess numerical robustness, mesh sensitivity was examined by progressively refining the mesh in the crack region through successive halving of the minimum allowed element size. Refinement continued until the difference in key response metrics—specifically, resonance frequency and peak normalised amplitude—between the finest mesh and the preceding refinement remained within 5%. This procedure ensured that the reported forced-response characteristics were not significantly influenced by discretisation effects.

The friction coefficient value of 0.1 lies within the range commonly reported for dry metal–metal contact under vibratory conditions, particularly for titanium alloys. Parametric variations within a broader range ($\mu = 0.05$–0.3) were examined at selected operating points and primarily influenced the magnitude of energy dissipation, whilst leaving the qualitative nonlinear signatures—such as amplitude-dependent frequency shift and normalised amplitude reduction—unchanged. A value of $\mu = 0.1$ was therefore adopted as a representative choice balancing physical realism and numerical stability.

Time-domain integration was performed using sufficiently small time steps to accurately resolve contact events during crack opening and closure. Additional checks confirmed that further reduction in the time step did not alter the steady-state response characteristics reported in this study, indicating that the results were not sensitive to the chosen integration parameters.

3.3. Case Definitions

Three cases were considered to systematically assess how variations in crack parameters affected the beam's nonlinear response. The baseline configuration featured a crack depth of b located at distance a from the free end (equivalently, a' from the clamped end). In the subsequent cases, a single parameter was varied relative to the baseline, as summarised in Table 1. These cases provided a structured framework for analysing the influence of crack depth and position on the forced response of the beam structure.

Table 1. Crack parameters for the representative beam in each case. Only one parameter is altered in each scenario to allow systematic comparison of the resulting nonlinearity.

Case	Crack Depth	Crack Position
Baseline	b	Distance a from free end (a' from clamp)
Case 1	$1.2\,b$	Same as baseline (deeper crack)
Case 2	b	Closer to the clamped end, $0.5\,a'$ (see Figure 2)

Baseline Case: The crack depth was b and it was positioned at distance a from the free end (equivalently, a' from the clamped end). This served as the reference configuration. For the baseline case, the geometric relations are:

$$4\,b = b' \quad , \quad 4\,a' = a \tag{1}$$

Case 1 (Deeper Crack): The crack depth was increased from b to $1.2\,b$, whilst its position remained unchanged (distance a from the free end). A deeper crack creates a larger compliance difference between the open and closed states, enabling more pronounced

stiffness variation during vibration cycles and strengthening the amplitude-dependent nonlinear behaviour.

Case 2 (Shifted Crack Location): The crack depth b remained the same, but the crack was repositioned closer to the clamped end at $0.5\,a'$. At that location, the moment created at the cracked cross section by both the excitation and inertia forces is larger, giving the crack greater influence on overall structural stiffness. This positioning affects how the crack opens and closes during vibration, influencing the breathing behaviour and consequently affecting the nonlinear response characteristics.

3.4. Nondimensionalisation of System Variables and Results

To facilitate comparison and enhance the generality of the results, the response quantities were nondimensionalised. The frequency was nondimensionalised by dividing the dimensional frequency by the first bending natural frequency, ω_n, of the baseline test case, neglecting contact between the crack surfaces. Thus, the nondimensional frequency is defined as:

$$\bar{\omega} = \frac{\omega}{\omega_n}. \tag{2}$$

The response amplitudes were measured at the free tip of the beam (where the excitation force was applied) and were nondimensionalised using a reference amplitude, $X_{0,\text{ref}}$. This reference amplitude was chosen as the static displacement that the beam tip exhibited under the applied force in each simulation. Accordingly, the nondimensional amplitude is:

$$\bar{X}_0 = \frac{X_0}{X_{0,\text{ref}}}, \tag{3}$$

where X_0 is the dimensional tip displacement amplitude.

Because $X_{0,\text{ref}}$ is the *static* displacement of the beam tip under the applied force, the nondimensional amplitude $\bar{X}_0$ represents the dynamic amplification factor at each frequency. At resonance, the amplification can be significantly greater than unity; a peak value of $\bar{X}_0 \approx 11.5$ indicates that the dynamic response amplitude is approximately 11.5 times the corresponding static deflection. This scaling is physically meaningful: the peak value reflects the effective quality factor (inverse of twice the damping ratio) of the system at resonance, and any deviation from overlapping normalised FRF curves between different forcing levels directly indicates amplitude-dependent (i.e., nonlinear) stiffness or damping.

For the excitation force, a natural scaling is provided by the characteristic inertial force of the system. Recognising that the linear stiffness is given by:

$$k = m\omega_n^2, \tag{4}$$

where m is the mass of the system, a reference force can be defined as:

$$F_{\text{ref}} = k\,X_{0,\text{ref}} = m\,\omega_n^2\,X_{0,\text{ref}}. \tag{5}$$

Accordingly, the nondimensional excitation force is defined as:

$$\bar{F} = \frac{F}{F_{\text{ref}}} = \frac{F}{m\,\omega_n^2\,X_{0,\text{ref}}}. \tag{6}$$

It is important to note that $X_{0,\text{ref}}$ varies for each forcing level, as it represents the static displacement under that specific applied force. Consequently, in a perfectly linear system, the nondimensional amplitude $\bar{X}_0$ would remain constant across all forcing levels, producing overlapping FRF curves.

4. Results and Discussion

In this section, three sets of FRF curves are examined for the baseline cracked beam and two modified crack configurations. The analysis reveals that the manifestation of crack-induced nonlinearity is strongly configuration-dependent: whilst certain crack parameters produce clearly identifiable nonlinear signatures, others yield quasi-linear response despite the presence of significant structural damage.

Figures 3–7 display the normalised amplitude $\bar{X}_0$ versus normalised frequency $\bar{\omega}$ for four nondimensional excitation forces: $\bar{F} = \{6.0, 12.0, 20.0, 30.0\}$. The FRF plots are presented over the range $\bar{\omega} = 0.8$–1.2, which encompasses the resonance region where amplitude-dependent nonlinear signatures—frequency shifts, peak broadening, and amplitude variations—are concentrated. At frequencies well below that range, the response amplitudes are small and all configurations behave quasi-linearly, providing no additional diagnostic information. Representative time-domain responses and their corresponding frequency spectra are also presented to illustrate the steady-state vibrational behaviour at near-resonance operating conditions, where nonlinear signatures are most pronounced. An intermediate forcing level of $\bar{F} = 7.5$ is selected for these time-domain illustrations, with the excitation frequency chosen close to the resonance of each respective configuration.

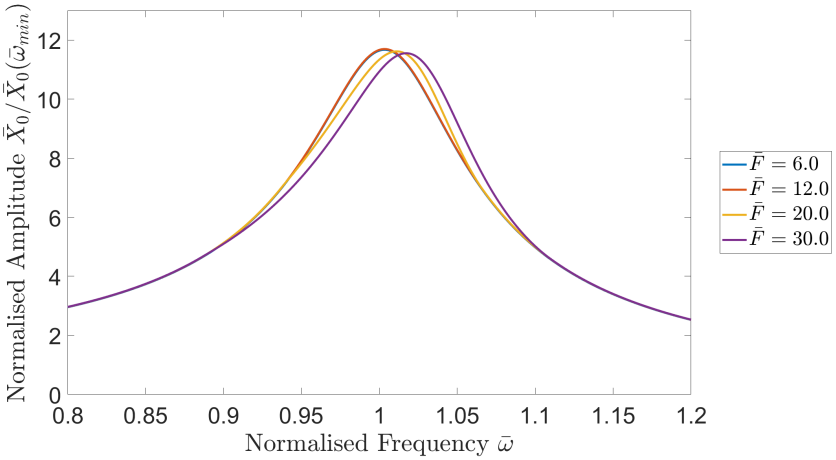

Figure 3. FRF for the baseline case (crack depth b, located at distance a from the free end). Normalised amplitude versus normalised frequency for $\bar{F} = 6.0, 12.0, 20.0, 30.0$.

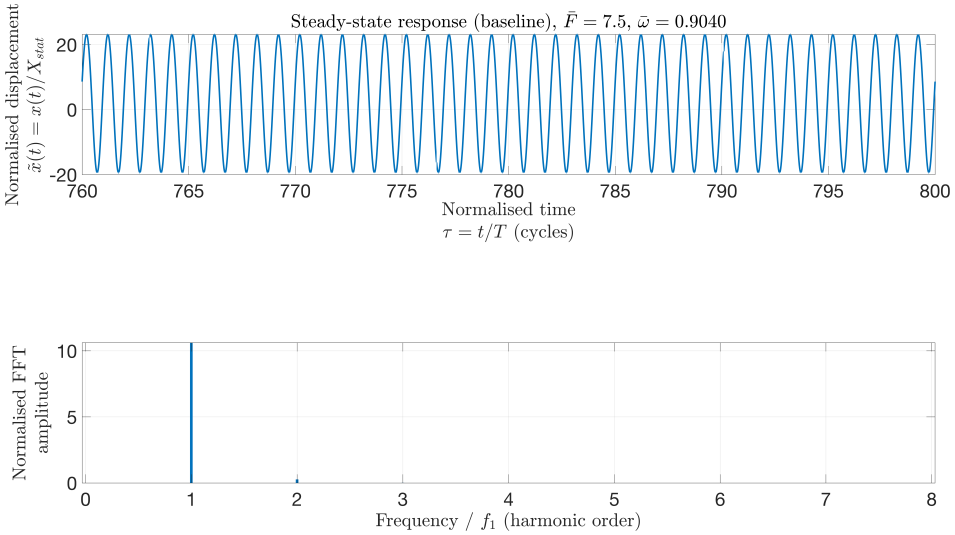

Figure 4. Steady-state time-domain response and frequency spectrum for the baseline case at $\bar{F} = 7.5$ and $\bar{\omega} = 0.9040$.

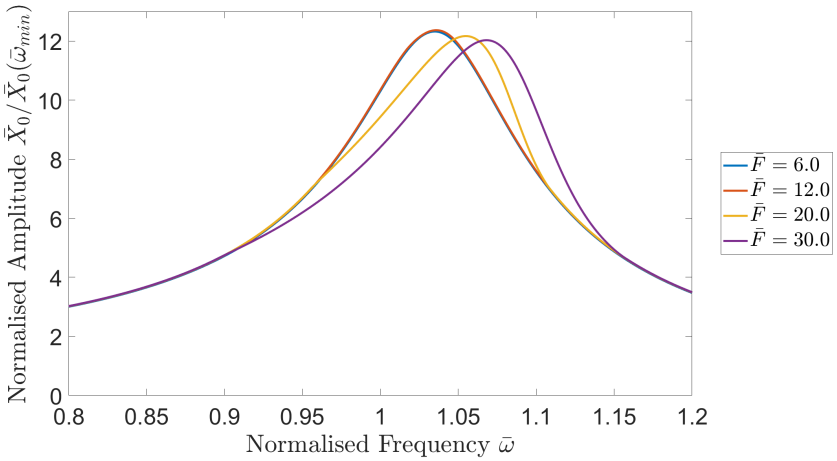

Figure 5. FRF for Case 1 with deeper crack (crack depth 1.2 b, located at distance a from the free end). Normalised amplitude versus normalised frequency for $\bar{F} = 6.0, 12.0, 20.0, 30.0$.

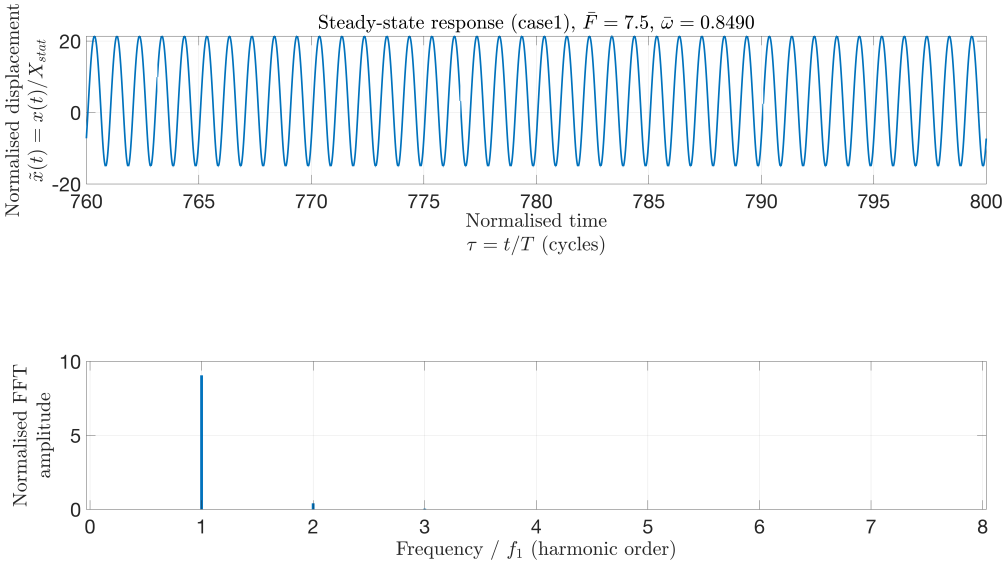

Figure 6. Steady-state time-domain response and frequency spectrum for Case 1 (deeper crack, 1.2 b) at $\bar{F} = 7.5$ and $\bar{\omega} = 0.8490$.

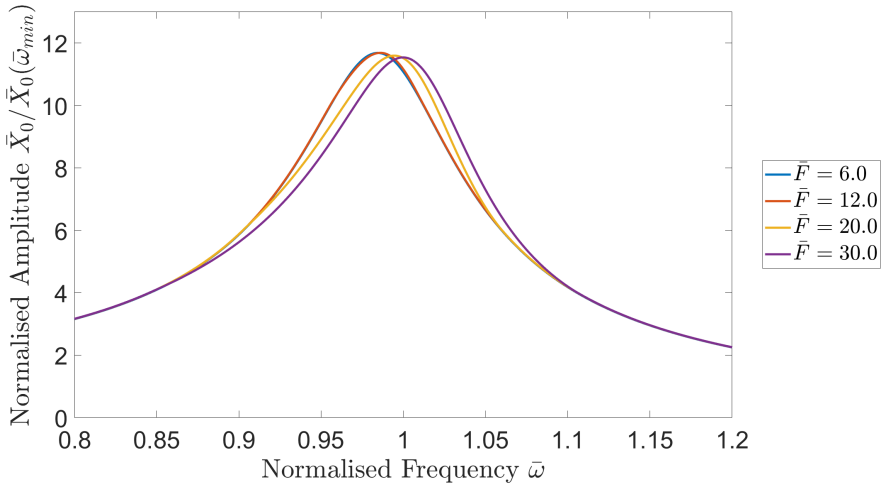

Figure 7. FRF for Case 2 with shifted crack location (crack depth b, located at 0.5 a' from the clamped end). Normalised amplitude versus normalised frequency for $\bar{F} = 6.0, 12.0, 20.0, 30.0$.

4.1. Baseline Case

Figure 3 presents the FRF for the baseline configuration, where the crack has depth b and is located at distance a from the free end. The response reveals remarkably weak nonlinearity across all forcing levels examined. All four curves exhibit resonance peaks at approximately $\bar{\omega} \approx 1.00$ with nearly identical normalised maximum amplitudes of approximately 11.5. The curves overlap almost completely throughout the entire frequency range, from the pre-resonance region through resonance and into the post-resonance regime.

The close overlap of all four FRF curves is an important observation that indicates quasi-linear behaviour. Since the amplitude normalisation accounts for the static displacement under each forcing level, an ideal linear system would be expected to produce closely overlapping curves; the physical response amplitude would scale approximately proportionally with force, and the normalised amplitude would remain relatively constant. The baseline configuration exhibits behaviour consistent with this expectation: examining the curves in detail, in the pre-resonance region ($\bar{\omega} < 0.95$), all four forcing levels produce very similar normalised amplitudes that increase gradually with frequency. At resonance ($\bar{\omega} \approx 1.00$), the peak amplitudes for all forcing levels cluster tightly around 11.5, with minimal variation. In the post-resonance region ($\bar{\omega} > 1.05$), the curves again overlap closely as amplitudes decay smoothly. The resonance peaks maintain symmetric, bell-shaped profiles with consistent bandwidth across all forcing levels, suggesting that the effective damping ratio remains approximately constant across the range of excitation amplitudes examined.

This behaviour suggests that the crack does not undergo significant breathing cycles that would introduce substantial amplitude-dependent stiffness or damping. At that location and with that crack depth, the vibrational motion appears insufficient to induce the intermittent crack closure and contact necessary for significant nonlinear effects to manifest. The crack surfaces may remain in near-continuous light contact throughout the vibration cycle, or conversely, remain predominantly open without sufficient compressive loading to force complete closure. In either scenario, the effective structural stiffness and damping appear to remain approximately constant across the forcing range examined. Without alternating between distinctly open and closed states with associated impact and friction, the system does not appear to develop the nonlinear damping mechanisms characteristic of breathing cracks, and consequently exhibits quasi-linear behaviour with closely overlapping FRF curves.

To further illustrate the steady-state response characteristics, Figure 4 shows the time-domain displacement and corresponding frequency spectrum at a near-resonance operating point ($\bar{F} = 7.5, \bar{\omega} = 0.9040$). This frequency is selected within the pre-resonance rise of the FRF, where the response amplification is substantial and any nonlinear effects would be most readily observable. The time-domain plot reveals a highly sinusoidal response with constant amplitude and frequency, displaying no visible distortion, modulation, or transient behaviour. The waveform maintains smooth, symmetric oscillations over the entire time window examined (cycles 760–800), confirming stable periodic motion.

The frequency spectrum provides complementary evidence of predominantly linear behaviour. A single dominant peak appears at the fundamental excitation frequency with normalised amplitude of approximately 10.5, consistent with the dynamic amplification expected near resonance. Notably, no significant higher harmonics are detectable in the spectrum: there are no visible peaks at integer multiples of the fundamental frequency. In nonlinear systems, even weakly nonlinear ones, energy transfer to higher harmonics typically produces visible spectral peaks. The absence of such peaks, combined with the relatively flat noise floor across all frequencies, suggests predominantly sinusoidal response characteristic of systems exhibiting quasi-linear behaviour.

4.2. Case 1: Deeper Crack

Figure 5 corresponds to Case 1, where the crack depth is increased from b to $1.2\,b$ whilst maintaining the same location. This configuration exhibits the strongest nonlinear effects among the three cases examined. At the lower forcing levels ($\bar{F} = 6.0$ and 12.0), the resonance occurs at approximately $\bar{\omega} \approx 1.00$ with peak normalised amplitudes of approximately 12.5. The two curves overlap closely, indicating quasi-linear behaviour at these moderate excitation levels; the physical response amplitude appears to scale approximately proportionally with force, consistent with the behaviour expected for a predominantly linear system.

However, at higher excitation levels, notable changes occur that indicate measurable nonlinear behaviour. At $\bar{F} = 20.0$, two significant phenomena emerge: first, the resonance peak shifts rightward to approximately $\bar{\omega} \approx 1.05$, representing approximately a 5% increase in resonance frequency; second, the peak normalised amplitude remains at approximately 12.5, similar to the lower forcing levels. At the highest forcing level $\bar{F} = 30.0$, the rightward frequency shift continues to $\bar{\omega} \approx 1.08$–$1.10$ (approximately 8–10% increase), and notably, the peak normalised amplitude decreases to approximately 12.0.

The rightward frequency shift is consistent with crack closure and stiffness restoration, i.e., an effective bilinear stiffness associated with opening–closing behaviour [72]. When the crack closes during the compressive phase of vibration, the crack surfaces are expected to come into contact and remain pressed together with friction (Coulomb friction coefficient $\mu = 0.1$), largely restoring the local stiffness towards near-intact values during portions of the vibration cycle. This intermittent stiffening appears to increase the system's effective natural frequency, manifesting as the rightward shift in resonance. The progressive nature of the shift—largely absent at $\bar{F} = 6.0$ and 12.0, appearing at $\bar{F} = 20.0$, and strengthening at $\bar{F} = 30.0$—indicates the amplitude-dependent nature of the effective stiffness. The magnitude of the shift provides an estimate of the stiffness variation between predominantly open and intermittently closed crack states: a 10% frequency shift corresponds to approximately 21% stiffness increase (since $\omega \propto \sqrt{k}$), suggesting that crack closure recovers a substantial fraction of the stiffness lost when the crack is open.

The reduction in normalised amplitude at $\bar{F} = 30.0$ provides important evidence of nonlinear damping mechanisms. In an ideal linear system, the normalised FRF curves would be expected to overlap closely regardless of forcing level, because both the physical response and the normalisation reference ($X_{0,\mathrm{ref}}$, the static displacement) would scale proportionally with force. The observation that the normalised amplitude decreases from approximately 12.5 (at $\bar{F} = 6.0$, 12.0, and 20.0) to approximately 12.0 (at $\bar{F} = 30.0$) suggests that the physical response amplitude is not increasing proportionally with the applied force. Whilst the actual physical amplitude at $\bar{F} = 30.0$ is larger than at lower forcing levels, its growth appears to be suppressed relative to linear scaling by enhanced energy dissipation mechanisms.

This amplitude reduction in normalised coordinates is consistent with nonlinear damping that appears to increase superlinearly with response amplitude. Two coupled mechanisms are likely to contribute to this enhanced dissipation. First, when the crack surfaces impact during closure, kinetic energy is dissipated through inelastic micro-deformations and local plasticity at the contact interface. The severity of these impacts—and thus the energy dissipation—is expected to increase with the relative velocity of the approaching surfaces, which grows with response amplitude. Second, once in contact, the crack surfaces remain pressed together under normal forces that increase with bending moment amplitude. Any relative tangential motion dissipates energy through Coulomb friction. At $\bar{F} = 30.0$, the higher response amplitude appears to lead to more severe impacts with greater relative velocities, longer expected contact durations, and higher

normal contact forces. These factors are expected to substantially increase the energy dissipation per cycle. This combined impact-friction damping appears to limit the growth of response amplitude, resulting in the observed decrease in normalised amplitude even though the physical amplitude continues to increase with forcing.

Examining the FRF curves in greater detail reveals additional features suggestive of nonlinearity. The curves for $\bar{F} = 6.0$ and 12.0 maintain symmetric, bell-shaped resonance peaks centred at $\bar{\omega} = 1.00$, characteristic of systems exhibiting predominantly linear behaviour. However, the curves for $\bar{F} = 20.0$ and 30.0 exhibit notably different characteristics. The resonance peaks shift rightward and become slightly asymmetric, with steeper slopes on the low-frequency side, behaviour characteristic of hardening-type nonlinearity where stiffness increases with amplitude. Furthermore, the bandwidth of the resonance peak increases noticeably for $\bar{F} = 30.0$, consistent with enhanced damping. In the pre-resonance region ($\bar{\omega} < 0.95$), all curves initially follow similar paths but begin to diverge as they approach resonance, with higher forcing levels developing slightly different gradients. In the post-resonance region ($\bar{\omega} > 1.15$), the curves appear to converge again, suggesting that nonlinear effects may diminish when operating away from resonance where vibrational amplitudes are smaller.

This behaviour indicates the activation of crack breathing nonlinearity at higher forcing amplitudes. The deeper crack (20% increase from b to 1.2 b) creates a larger compliance variation between open and closed states. At low forcing levels ($\bar{F} = 6.0$ and 12.0), the vibrational amplitude appears insufficient to fully close the crack during the compressive phase of oscillation. The crack appears to remain predominantly open with reduced but approximately constant stiffness throughout the cycle, producing behaviour consistent with a predominantly linear system as evidenced by the closely overlapping FRF curves. However, at $\bar{F} = 20.0$ and 30.0, the increased response amplitude appears to drive the crack surfaces into contact during each compressive phase, initiating the nonlinear breathing mechanism. The response characteristics are consistent with the crack alternating between open (reduced stiffness) and closed (restored stiffness) states, producing amplitude-dependent effective stiffness. Simultaneously, the contact and separation events dissipate energy through impact and friction, introducing amplitude-dependent damping that appears to suppress response growth.

The time-domain response for Case 1, shown in Figure 6 at $\bar{F} = 7.5$ and $\bar{\omega} = 0.8490$, reveals relatively clean periodic motion. The excitation frequency is selected near Case 1's resonance, which occurs at a lower normalised frequency than the baseline owing to the deeper crack's greater compliance in the predominantly open state. The waveform remains reasonably smooth and sinusoidal, though close inspection reveals mild asymmetry between positive and negative half-cycles, consistent with the bilinear stiffness character of the breathing crack. The periodicity and stability indicate steady-state behaviour despite the presence of contact nonlinearity.

The frequency spectrum remains dominated by the fundamental component at the excitation frequency, with a normalised amplitude of approximately 9.0. This is noticeably lower than the baseline case (approximately 10.5 in Figure 4 at a comparable near-resonance condition), providing evidence of enhanced energy dissipation due to the deeper crack's more active breathing. A small but discernible second harmonic is visible in the spectrum, indicating that the bilinear opening–closing mechanism generates some higher-frequency content even at this moderate forcing level. The presence of this harmonic component, absent in the baseline spectrum, provides direct spectral evidence of the nonlinear stiffness variation introduced by the deeper crack's breathing cycles. This is consistent with the expected physical mechanism: near resonance, the larger vibra-

tional amplitudes promote more vigorous crack opening–closing cycles, producing both enhanced damping and measurable harmonic distortion in the response.

4.3. Case 2: Shifted Crack Location

Figure 7 shows the FRF for Case 2, where the crack depth is maintained at b but is relocated closer to the clamped end at position $0.5\,a'$. Similar to the baseline case, this configuration exhibits remarkably weak nonlinearity despite the crack's repositioning to a region experiencing larger moments. All four curves are nearly indistinguishable, with resonance peaks occurring at approximately $\bar{\omega} \approx 1.00$ and peak normalised amplitudes of approximately 11.5–12.0 across all forcing levels.

The close overlap of all four FRF curves indicates quasi-linear behaviour, analogous to the baseline case. Since the amplitude normalisation accounts for the static displacement under each forcing level, this overlap suggests that the physical response amplitude scales approximately linearly with force; there appears to be minimal amplitude-dependent stiffness or damping variation. Examining the curves in detail: in the pre-resonance region ($\bar{\omega} < 0.95$), all curves follow very similar paths; at resonance ($\bar{\omega} \approx 1.00$), the peak amplitudes span a narrow range of approximately 11.5–12.0 with no apparent systematic trend with forcing level; and in the post-resonance region ($\bar{\omega} > 1.05$), the curves again overlap closely. The resonance peaks maintain symmetric, bell-shaped profiles with consistent bandwidth across all forcing levels, suggesting approximately constant effective damping.

Moreover, the peak normalised amplitudes in Case 2 (11.5–12.0) are marginally higher than in the baseline case (approximately 11.5), suggesting that the crack closer to the clamped boundary produces slightly greater overall compliance. This is consistent with the crack being located in a region of higher bending moment, where it has greater influence on the beam's global stiffness. For a cantilever beam, the bending moment varies linearly from zero at the free end to maximum at the clamped end. Positioning the crack at $0.5\,a'$ (closer to the clamp) places it in a region experiencing approximately double the moment compared to the baseline position at a for the same tip deflection. However—and this is important—this enhanced compliance appears to remain relatively constant across all forcing levels, as evidenced by the overlapping FRF curves. There is no observable amplitude-dependent stiffness variation that would cause the curves to separate.

The quasi-linear behaviour in this configuration appears to result from the crack's proximity to the clamped boundary and the associated mechanical environment. At that location, the moment created at the cross section where the crack is located—by both the excitation and inertia forces—is larger, giving the crack more influence on overall structural stiffness. This enhanced influence appears to make the crack open and close more readily in response to the oscillating bending moment. Even at low forcing levels, the response is consistent with the crack undergoing complete breathing cycles. However—and this is the crucial distinction from Case 1—because the crack appears to breathe readily even at lower forcing levels, the stiffness reduction appears to remain relatively limited across the examined forcing range. The crack does not appear to require high excitation amplitudes to activate breathing; it appears to breathe at all forcing levels examined. Consequently, no strong amplitude-dependent stiffness variation appears to develop, and the system operates with almost constant (though reduced) effective stiffness and damping.

Without significant variation in stiffness or damping between different forcing levels, the system exhibits quasi-linear response with no observable frequency shift and no reduction in normalised amplitude. The crack's location closer to the clamp, where the moment created at the cracked cross section has greater influence on overall stiffness, appears to prevent the development of significant amplitude-dependent nonlinearity. The crack ap-

pears to breathe readily at all forcing levels, maintaining approximately constant reduced stiffness and damping that prevent distinctive nonlinear phenomena from manifesting in the FRF.

This finding suggests that crack-induced nonlinearity depends not only on crack depth but also critically on the crack's position relative to the moment distribution along the beam. A crack in a moderate-moment region (like the baseline position, distance a from the free end) with sufficient depth (as in Case 1) can develop measurable amplitude-dependent breathing as forcing increases, because it appears to transition from a quasi-linear regime (crack predominantly open) at low forcing to a nonlinear regime (crack undergoes full breathing with impact and high contact forces) at high forcing. However, a crack closer to the support, where the moment has greater influence, may breathe readily across the entire forcing range examined, maintaining approximately constant effective properties and producing quasi-linear response despite the presence of active crack breathing.

The time-domain response for Case 2, presented in Figure 8, is consistent with this quasi-linear behaviour. At $\bar{F} = 7.5$ and $\bar{\omega} = 0.9040$, the displacement exhibits a predominantly sinusoidal pattern with smooth, symmetric oscillations. The waveform shows no readily visible distortion, suggesting that crack breathing does not introduce significant nonlinear effects at that operating condition.

The frequency spectrum shows a single dominant fundamental component with normalised amplitude of approximately 10.5, nearly identical to the baseline case (Figure 4) and noticeably higher than Case 1 (approximately 9.0, Figure 6). This comparison is noteworthy: the observation that Case 2 and baseline produce similar spectral amplitudes whilst Case 1 shows reduced amplitude suggests that Case 2 does not develop the enhanced nonlinear damping mechanisms that appear to characterise Case 1. The second harmonic component visible in Case 1's spectrum is absent here, further confirming that the shifted crack location does not produce the same degree of nonlinear harmonic generation. The similarity between Case 2 and baseline frequency spectra suggests that repositioning the crack closer to the clamp does not activate the amplitude-dependent damping observed in the deeper crack configuration.

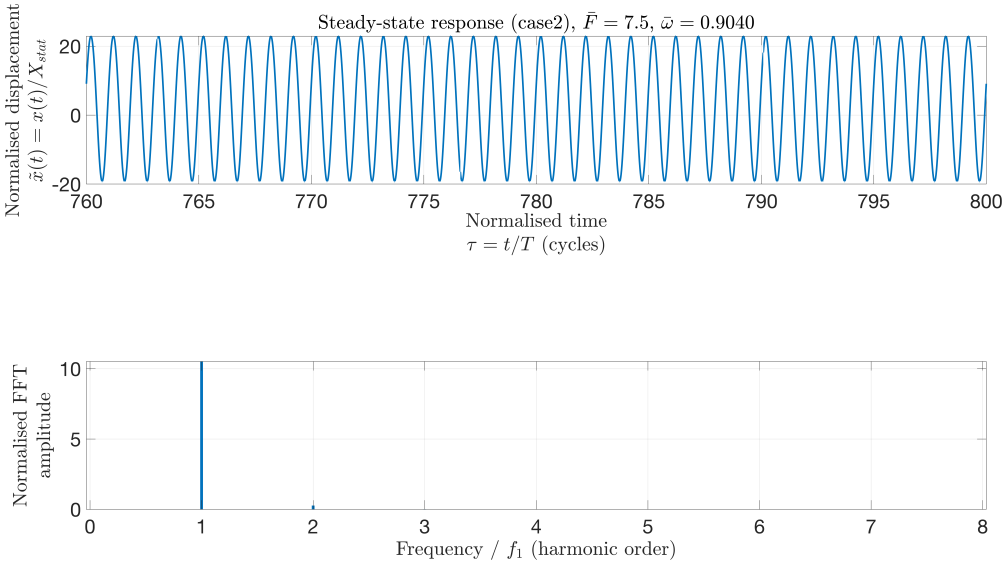

Figure 8. Steady-state time-domain response and frequency spectrum for Case 2 (shifted crack location, $0.5\,a'$) at $\bar{F} = 7.5$ and $\bar{\omega} = 0.9040$.

4.4. Overall Observations and Discussion

The comparative analysis of the three configurations reveals that crack-induced nonlinearity in forced vibration is subtle and highly sensitive to the specific combination of crack parameters and operating conditions. The normalised FRF presentation is particularly effective for exposing this configuration dependence: two of the three cases examined exhibit quasi-linear behaviour across all forcing levels despite the presence of significant crack damage, whilst the third produces measurable but moderate nonlinear signatures only at elevated forcing.

1. **Crack depth appears to govern the threshold for nonlinear behaviour:** Only Case 1, with the deeper crack ($1.2\,b$), exhibits significant departure from quasi-linear behaviour, specifically, rightward frequency shifts and reduction in normalised amplitude at high forcing levels. The 20% increase in crack depth from b to $1.2\,b$ appears sufficient to cross a critical threshold, transforming the system from quasi-linear (closely overlapping FRF curves) to measurably nonlinear (separated curves with frequency-dependent and amplitude-dependent behaviour). The deeper crack creates a larger compliance difference between open and closed states: when open, the 20% deeper crack reduces local stiffness more substantially; when closed, both cracks appear to return to similar near-intact stiffness. This amplified compliance variation appears to enable the development of amplitude-dependent effective stiffness as forcing increases. The baseline and Case 2, both with crack depth b, show close overlap of FRF curves across all forcing levels examined ($\bar{F}$ up to 30.0), suggesting that physical response amplitudes scale approximately linearly with force. This suggests a threshold crack depth may exist below which breathing effects, whilst potentially present, do not produce sufficient stiffness or damping variation to cause readily detectable nonlinearity in the forced response. This threshold likely depends on the ratio of crack depth to total cross-sectional height and on the local moment and displacement amplitudes at the crack location.
2. **Frequency shift provides quantitative indication of amplitude-dependent stiffness restoration:** The rightward shift of resonance frequency in Case 1 at higher forcing levels ($\bar{F} = 20.0$ and 30.0) provides quantitative evidence consistent with crack closure restoring structural stiffness in an amplitude-dependent manner. At $\bar{F} = 6.0$ and 12.0, the resonance frequency remains at approximately $\bar{\omega} \approx 1.00$, similar to the baseline case, suggesting the crack remains predominantly open with approximately constant reduced stiffness. At $\bar{F} = 20.0$, the resonance shifts to approximately $\bar{\omega} \approx 1.05$ (approximately 5% increase), indicating that crack closure begins to significantly affect system dynamics. At $\bar{F} = 30.0$, the shift reaches approximately $\bar{\omega} \approx 1.10$ (approximately 10% increase). Since resonance frequency scales as $\omega_n \propto \sqrt{k/m}$, this 10% frequency increase corresponds to approximately 21% effective stiffness increase, suggesting that intermittent crack closure recovers a substantial fraction of the stiffness lost when the crack is fully open. The progressive nature of this shift with increasing forcing amplitude indicates the strongly amplitude-dependent character of the effective stiffness, a characteristic feature of geometric nonlinearity arising from the bilinear (open/closed) nature of crack stiffness. The absence of observable frequency shift in the baseline case and Case 2 across all forcing levels provides clear contrast, suggesting that the shift in Case 1 represents genuine physical nonlinearity rather than numerical artifact. This frequency shift signature could potentially serve as a practical diagnostic tool for breathing crack detection in structural health monitoring applications.
3. **Normalised amplitude reduction provides evidence of nonlinear damping:** The reduction in normalised amplitude observed in Case 1 at $\bar{F} = 30.0$ (peak amplitude ap-

proximately 12.0) compared to lower forcing levels (peak amplitude approximately 12.5) represents perhaps one of the most distinctive signatures of breathing crack nonlinearity. This approximately 4% reduction in normalised amplitude is particularly significant because the normalisation procedure explicitly accounts for the scaling of static displacement with force. In an ideal linear system, normalised FRF curves would be expected to overlap closely; the physical response would scale proportionally with force, as would the normalisation reference $X_{0,\text{ref}}$, causing the normalised response to remain approximately constant. The observation that the normalised amplitude decreases at the highest forcing level suggests that the physical response amplitude, whilst still increasing with force, is not increasing proportionally. The response growth appears to be suppressed by nonlinear damping mechanisms that appear to increase superlinearly with response amplitude.

Two coupled physical mechanisms are likely to contribute to this enhanced dissipation. When crack surfaces impact during closure, kinetic energy is dissipated through inelastic deformation, local plasticity, and acoustic radiation at the contact interface. The energy dissipated per impact event is expected to increase with the square of the relative impact velocity (kinetic energy), which itself increases with response amplitude. Once in contact, frictional sliding between surfaces pressed together dissipates energy at a rate proportional to the normal contact force (which increases with bending moment amplitude) and the relative sliding velocity (which increases with response amplitude). At $\bar{F} = 30.0$, the combination of higher impact velocities, longer expected contact durations, and higher normal contact forces appears to cause energy dissipation to increase superlinearly with response amplitude. This nonlinear damping appears to limit response growth, resulting in the observed decrease in normalised amplitude even as physical amplitude continues to increase. The baseline and Case 2 configurations show minimal such amplitude reduction—their normalised peak amplitudes remain approximately constant across all forcing levels—suggesting this is a distinctive feature of activated breathing nonlinearity rather than a general characteristic of cracked structures.

4. **Location relative to moment distribution appears to govern breathing character and nonlinear activation:** Case 2's quasi-linear behaviour (closely overlapping FRF curves), contrasted with Case 1's measurable nonlinearity (separated curves, frequency shift, amplitude reduction), suggests that crack location is as important as crack depth in determining whether nonlinear signatures manifest in the forced response. Both baseline and Case 2 configurations have identical crack depth (b), yet their positions along the beam appear to produce different global compliance and different breathing characteristics. Case 2, positioned at $0.5\,a'$ (closer to the clamp), experiences approximately double the bending moment compared to the baseline position (distance a from the free end) for the same tip deflection. This larger moment gives the crack greater influence on overall structural stiffness, evident from Case 2's marginally higher peak normalised amplitudes (11.5–12.0) compared to baseline (approximately 11.5), indicating greater global compliance. However, the larger moment also appears to mean the crack breathes readily even at low forcing levels. The observed response is consistent with the crack undergoing complete open–close cycles across the entire forcing range examined, maintaining relatively constant (though reduced) effective stiffness and damping at all forcing levels. This appears to prevent the development of amplitude-dependent properties, the key to nonlinear signature generation. In contrast, the baseline configuration at distance a' from the clamp experiences smaller moments and also shows quasi-linear behaviour, but possibly for a different reason: the crack depth may be insufficient to create sig-

nificant stiffness variation even when it does breathe, and the moderate moment may not drive full closure except possibly at the very highest forcing levels. Case 1, with sufficient crack depth (1.2 b) at the baseline location (distance a from the free end), appears to achieve a favourable combination: moderate moment that increases with forcing amplitude, combined with sufficient crack depth to create large stiffness variation between open and closed states, and sufficient displacement amplitude to drive severe impacts and high contact forces at high forcing levels. This combination appears to enable the crack to transition from quasi-linear behaviour (predominantly open, minimal contact) at low forcing to measurably nonlinear behaviour (full breathing with impacts and friction) at high forcing, producing the distinctive signatures observed in the FRF. The key physical insight is that observable nonlinearity appears to require not just crack breathing, but amplitude-dependent variation in breathing severity: either the crack must transition from not breathing to breathing as amplitude increases (baseline with deeper crack), or from gentle breathing to severe breathing with high-force impacts (not observed in present configurations). Case 2 appears to breathe readily across all forcing levels but without sufficient variation in contact severity, whilst the baseline and Case 2 with shallow cracks do not appear to develop sufficient compliance variation.

These results suggest that observable crack-induced nonlinearity in normalised FRF curves requires a specific and restrictive combination of sufficient crack depth (to enable large compliance variation between open and closed states), appropriate positioning relative to moment distribution (to achieve amplitude-dependent variation in breathing severity rather than constant breathing), and adequate forcing amplitude (to drive the transition from quasi-linear to nonlinear regimes). Crucially, the parametric study demonstrates that this combination is not easily achieved: two of the three configurations examined—representing different but physically realistic crack scenarios—produce no readily detectable nonlinear signatures despite the presence of active crack damage. The normalised FRF presentation provides an effective framework for interpreting these results: closely overlapping curves indicate quasi-linear behaviour with minimal amplitude-dependent effects, whilst separated curves with rightward frequency shifts and reduced normalised amplitudes provide evidence of activated breathing nonlinearity with amplitude-dependent stiffness and damping. The central implication for structural health monitoring is that the absence of nonlinear signatures in vibration-based testing does not imply the absence of damage. Understanding which crack configurations produce detectable nonlinear signatures, and under what forcing conditions, is therefore essential for designing effective and reliable monitoring protocols.

4.5. Implications for Structural Health Monitoring

From a structural health monitoring perspective, these findings reveal both opportunities and challenges with direct implications for practical implementation, particularly when viewed through the lens of normalised FRF analysis.

The clear separation of FRF curves in Case 1 at higher forcing levels—manifesting as a rightward frequency shift and reduction in normalised amplitude—provides diagnostic signatures for breathing crack detection that are fundamentally different from conventional linear modal analysis approaches. The key insight is that these signatures appear to arise from amplitude-dependent nonlinear behaviour: the effective stiffness and damping change as a function of response amplitude. Monitoring how the resonance frequency and normalised peak amplitude vary with excitation level, rather than measuring them at a single amplitude, may reveal breathing cracks through their distinctive nonlinear response. For Case 1, the approximately 10% rightward frequency shift and approximately 4% nor-

malised amplitude reduction between low and high forcing represent measurable signals, though their moderate magnitude underscores the subtlety of breathing crack nonlinearity and the need for carefully designed testing protocols to reliably detect such signatures.

However, the quasi-linear behaviour of the baseline and Case 2 configurations—evidenced by closely overlapping FRF curves across all forcing levels—highlights a significant challenge: cracks of moderate depth (baseline) or positioned where they appear to breathe readily across the forcing range (Case 2) may produce minimal detectable nonlinearity in vibration-based testing. These configurations would appear as simple stiffness reductions in linear modal tests (evident from marginally higher normalised amplitudes indicating greater compliance), but without the distinctive nonlinear signatures that enable confident crack detection. Traditional frequency-based monitoring techniques relying on natural frequency changes would likely observe only the small overall frequency reduction due to reduced average stiffness but would miss the crack's breathing character entirely if only single-amplitude testing were performed. The baseline case, with FRF curves that are very similar across forcing levels, would appear predominantly quasi-linear in vibration tests, suggesting important limitations of conventional approaches for detecting certain breathing crack configurations.

This suggests the potential need for multi-faceted monitoring strategies incorporating amplitude-dependent testing:

- **Multi-amplitude swept-sine testing protocols:** Rather than testing at a single excitation amplitude, protocols could systematically vary forcing amplitude and monitor changes in resonance frequency and normalised peak response. The appearance of frequency shifts and normalised amplitude changes as forcing increases may provide evidence of breathing behaviour. For Case 1, distinctive signatures emerge between $\bar{F} = 12.0$ and 20.0, suggesting that testing across a range spanning at least a factor of 2–3 in forcing amplitude may be necessary to activate and detect nonlinear behaviour. Care must be taken to ensure excitation levels are sufficient to activate breathing without inducing further damage or exceeding operational stress limits.
- **Normalised FRF analysis as diagnostic tool:** The normalisation procedure employed in this study—scaling amplitude by static displacement under the applied force—provides particularly clear visualisation of nonlinear effects. In ideal linear systems, normalised FRF curves would be expected to overlap closely; significant separation may indicate nonlinear behaviour. This provides a relatively simple visual diagnostic: closely overlapping curves across forcing levels indicate quasi-linear response, whilst separated curves indicate amplitude-dependent nonlinearity. The direction of separation may provide additional information: a rightward frequency shift indicates hardening (stiffness restoration through crack closure), whilst normalised amplitude reduction indicates enhanced nonlinear damping (energy dissipation through contact).
- **Advanced nonlinear identification techniques:** Beyond simple resonance tracking, techniques such as backbone curve extraction (plotting resonance frequency versus response amplitude), nonlinear modal analysis, and restoring force surface methods can characterise amplitude-dependent stiffness and damping. The results suggest that for breathing cracks, frequency shift may be a more sensitive indicator than amplitude reduction (Case 1 shows a frequency shift of approximately 10% versus an amplitude reduction of approximately 4%), so techniques focused on tracking stiffness variation may be particularly effective.
- **Multi-modal testing across different mode shapes:** The present study examined only the first bending mode. Higher modes produce different displacement and moment distributions along the beam, potentially activating breathing in cracks that appear quasi-linear in the first mode. A crack positioned near a node of the first

mode might show minimal breathing in first-mode testing but potentially stronger breathing in second- or third-mode testing. Comprehensive monitoring may require examining multiple modes at multiple amplitude levels.

- **Complementary non-vibrational inspection methods:** The results suggest that certain crack configurations (baseline and Case 2) produce minimal nonlinear signatures in vibration testing despite representing significant structural compromise (20% depth penetration). Vibration-based methods alone may be insufficient for detecting all critical crack configurations. Integration with complementary techniques—ultrasonic inspection, eddy current testing, thermography, or visual inspection—may provide more robust damage detection. Thermography during vibrational excitation might reveal localised heating at crack interfaces due to frictional dissipation, providing an alternative detection mechanism for cracks that produce minimal amplitude-dependent behaviour.

For aerospace applications, these results suggest that structural health monitoring systems should be carefully designed with knowledge of likely crack initiation sites and their relationship to vibrational mode shapes and moment distributions. Components could be assessed to identify critical regions where cracks would be most difficult to detect through vibration-based methods, for example, regions analogous to Case 2 where high moments may cause ready breathing across all forcing levels, potentially masking amplitude-dependent signatures. These regions may require enhanced local monitoring or more frequent direct inspection. Relying solely on passive vibration monitoring at operational levels may be insufficient if operational loads do not span a sufficient range to reveal amplitude-dependent behaviour. Active excitation testing at controlled amplitude levels, systematically varied to reveal nonlinear signatures, may be beneficial for reliable crack detection. The frequency shift and normalised amplitude reduction observed in Case 1 provide potential target signatures for detection algorithms, but the variability in signatures across crack configurations suggests the need for adaptive, multi-parameter approaches rather than simple threshold-based methods.

5. Conclusions

This study presented a numerical investigation into the forced vibrational response of cracked beam structures representing aerospace components using VIBRANT, a time-marching finite element platform. Representative cantilever beams with varying crack configurations were analysed under harmonic excitation to characterise the conditions under which breathing crack nonlinearity produced detectable signatures, and equally importantly, the conditions under which it did not.

The parametric investigation revealed that crack-induced nonlinearity was subtle and strongly configuration-dependent, requiring specific combinations of crack depth, location relative to moment distribution, and excitation amplitude to produce measurable signatures. The deeper crack configuration (Case 1, 1.2 b) exhibited amplitude-dependent behaviour at higher forcing levels, manifesting as rightward resonance frequency shifts (approximately 10% from $\bar{\omega} \approx 1.00$ to $\bar{\omega} \approx 1.10$) and normalised amplitude reductions of approximately 4%. These moderate but measurable phenomena resulted from crack closure restoring structural stiffness and enhanced energy dissipation through impact-friction damping. In contrast, both the baseline configuration and the repositioned crack (Case 2) exhibited quasi-linear behaviour across all forcing levels examined, with closely overlapping normalised FRF curves, despite representing significant structural compromise. The repositioned crack's proximity to the clamped boundary caused ready breathing across the entire forcing range, maintaining relatively constant effective properties that prevented distinctive nonlinear signatures from developing.

These findings highlight important challenges for structural health monitoring. The diagnostic signatures in Case 1—rightward frequency shift coupled with normalised amplitude reduction—provide promising indicators for breathing crack detection, but their moderate magnitude and strict dependence on crack configuration underscore the difficulty of relying solely on nonlinear vibration signatures for damage detection. Cracks of moderate depth or positioned where moment distribution causes ready breathing may produce minimal detectable nonlinearity, potentially evading conventional vibration-based monitoring. This suggests the need for carefully designed monitoring strategies incorporating multi-amplitude testing protocols, advanced nonlinear identification techniques, and multi-modal testing.

The results demonstrate VIBRANT's capability to capture the full spectrum of crack breathing dynamics, from quasi-linear response where nonlinear signatures are absent to measurable amplitude-dependent effects where they emerge. The normalised FRF presentation proves particularly effective for exposing this configuration-dependence: closely overlapping curves indicate quasi-linear response, whilst separated curves with specific patterns provide evidence of activated breathing nonlinearity. Future work should focus on extending the analysis to more complex crack geometries, multiple crack configurations, and realistic three-dimensional aerospace component geometries. Experimental validation of the predicted configuration-dependent behaviour—particularly the conditions under which nonlinear signatures appear and disappear—remains important for establishing confidence in these computational predictions and refining damage detection protocols. Additionally, investigation of higher excitation levels and broader parametric ranges could establish quantitative thresholds for crack detectability based on depth, location, and operational conditions, ultimately contributing to improved safety and reliability of aerospace structures.

Funding: This research received no external funding.

Data Availability Statement: The authors declare no data were generated for this research apart from those presented in this paper.

Acknowledgments: Mertol Tüfekci would like to thank Serhat Arda Şahin and the Composite Materials Laboratory in the Faculty of Mechanical Engineering of Istanbul Technical University (https://mkn.itu.edu.tr/en/research/laboratories/katicisimlerinmekanigiEski/composite-materials-laboratory, accessed on 28 February 2026) for their valuable technical support contributing to this research.

Conflicts of Interest: The author declares they have no known conflicts of interest related to this research.

References

1. Tüfekci, M. Performance evaluation analysis of Ti-6Al-4V foam fan blades in aircraft engines: A numerical study. *Compos. Part C Open Access* **2023**, *12*, 100414. https://doi.org/10.1016/j.jcomc.2023.100414.
2. Tufekci, M.; Rendu, Q.; Yuan, J.; Dear, J.P.; Salles, L.; Cherednichenko, A.V. *Stress and Modal Analysis of a Rotating Blade and the Effects of Nonlocality*; American Society of Mechanical Engineers: New York, NY, USA, 2020; Volume 10B-2020, pp. 1–12. https://doi.org/10.1115/GT2020-14821.
3. Koç, H.; Ömer Ekim Genel.; Tüfekci, M.; Tüfekci, E. Analysis of the dynamical behaviour of spinning annular disks with various boundary conditions. *Mech. Based Des. Struct. Mach.* **2023**, *51*, 5427–5451. https://doi.org/10.1080/15397734.2021.1999269.
4. Petrov, E.P.; Ewins, D.J. State-of-the-art dynamic analysis for non-linear gas turbine structures. *Proc. Inst. Mech. Eng. Part G J. Aerosp. Eng.* **2004**, *218*, 199–211. https://doi.org/10.1243/0954410041872906.
5. Barreau, V.; Denimal, E.; Salles, L. Topological Optimisation and 3D Printing of a Bladed Disc. In Proceedings of the ASME Turbo Expo, Rotterdam, The Netherlands, 13–17 June 2022; Volume 8-A. https://doi.org/10.1115/GT2022-78141.

6. Denimal, E.; El Haddad, F.; Wong, C.; Salles, L. Topological optimization of under-platform dampers with moving morphable components and global optimization algorithm for nonlinear frequency response. *J. Eng. Gas Turbines Power* **2021**, *143*, 021021. https://doi.org/10.1115/GT2020-14394.
7. Sun, Y.; Yuan, J.; Salles, L. Flutter analysis of blisks with friction ring dampers. In Proceedings of the Global Power and Propulsion Society, Xi'an, China, 11–13 April 2022. https://doi.org/10.33737/gpps21-tc-42.
8. Tüfekci, M. Forced Vibration Analysis of Rotating Blades Subjected to Large Deformations: A Numerical Investigation with VIBRANT. In *Proceedings of the ASME 2025 Aerospace Structures, Structural Dynamics, and Materials Conference*; American Society of Mechanical Engineers: New York, NY, USA, 2025, pp. 1–10. https://doi.org/10.1115/SSDM2025-152240.
9. LaBryer, A.; Attar, P. A harmonic balance approach for large-scale problems in nonlinear structural dynamics. *Comput. Struct.* **2010**, *88*, 1002–1014. https://doi.org/10.1016/j.compstruc.2010.06.003.
10. Krack, M.; Gross, J. *Harmonic Balance for Nonlinear Vibration Problems*; Springer: Berlin/Heidelberg, Germany, 2019; p. 159.
11. Cao, L.; Chen, Y.; Wang, L.; Salles, L.; Zheng, Z. Perturbation Function Iteration Method: A New Framework for Solving Periodic Solutions of Non-linear and Non-smooth Systems. *arXiv* **2025**, arXiv:2510.23071.
12. Li, Y.; Zheng, Z. Uncertainty quantification of nonlinear vibration response of the oscillator with double-sided unilateral spring. *AIP Adv.* **2023**, *13*, 105324. https://doi.org/10.1063/5.0175313.
13. Alijani, F.; Amabili, M.; Balasubramanian, P.; Carra, S.; Ferrari, G.; Garziera, R. Damping for large-amplitude vibrations of plates and curved panels, Part 1: Modeling and experiments. *Int. J. Non-Linear Mech.* **2016**, *85*, 23–40. https://doi.org/10.1016/j.ijnonlinmec.2016.05.003.
14. Fereidoon, A.; Ghadimi, M.; Barari, A.; Kaliji, H.D.; Domairry, G. Nonlinear Vibration of Oscillation Systems using Frequency-Amplitude Formulation. *Shock Vib.* **2012**, *19*, 323–332. https://doi.org/10.3233/SAV-2010-0633.
15. Vitanov, N.K.; Hoffmann, N.P.; Wernitz, B. Nonlinear time series analysis of vibration data from a friction brake: SSA, PCA, and MFDFA. *Chaos, Solitons Fractals* **2014**, *69*, 90–99. https://doi.org/10.1016/J.CHAOS.2014.09.010.
16. Masri, S.F.; Miller, R.K.; Saud, A.F.; Caughey, T.K. Identification of Nonlinear Vibrating Structures: Part II—Applications. *J. Appl. Mech.* **1987**, *54*, 923–929. https://doi.org/10.1115/1.3173140.
17. Chen, G.X.; Zhou, Z.R. Time–frequency analysis of friction-induced vibration under reciprocating sliding conditions. *Wear* **2007**, *262*, 1–10. https://doi.org/10.1016/J.WEAR.2006.03.055.
18. Karkar, S.; Cochelin, B.; Vergez, C. A high-order purely frequency-based harmonic balance approach for continuation of periodic solutions in non-smooth dynamical systems. *J. Sound Vib.* **2014**, *333*, 2557–2577. https://doi.org/10.1016/j.jsv.2014.06.025.
19. Tüfekci, M. Development and Application of a High-Fidelity Numerical Tool for Dynamic Analysis of Bladed Disc Systems with Underplatform Dampers in Aircraft Engine Turbines. In *Proceedings of the Volume 10B: Structures and Dynamics—Fatigue, Fracture, and Life Prediction; Probabilistic Methods; Rotordynamics; Structural Mechanics and Vibration*; American Society of Mechanical Engineers: New York, NY, USA, 2024, pp. 1–13. https://doi.org/10.1115/GT2024-123318.
20. Bonello, P.; Hai, P.M. A receptance harmonic balance technique for the computation of the vibration of a whole aero-engine model with nonlinear bearings. *J. Sound Vib.* **2009**, *324*, 221–242. https://doi.org/10.1016/J.JSV.2009.01.039.
21. Akbarzade, M.; Farshidianfar, A. Nonlinear transversely vibrating beams by the improved energy balance method and the global residue harmonic balance method. *Appl. Math. Model.* **2017**, *45*, 393–404. https://doi.org/10.1016/J.APM.2017.01.002.
22. Pesaresi, L.; Salles, L.; Jones, A.; Green, J.S.; Schwingshackl, C.W. Modelling the nonlinear behaviour of an underplatform damper test rig for turbine applications. *Mech. Syst. Signal Process.* **2017**, *85*, 662–679. https://doi.org/10.1016/j.ymssp.2016.09.007.
23. Sanliturk, K.Y.; Ewins, D.J.; Stanbridge, A.B. Underplatform dampers for turbine blades: Theoretical modeling, analysis, and comparison with experimental data. *J. Eng. Gas Turbines Power* **2001**, *123*, 919–929. https://doi.org/10.1115/1.1385830.
24. Ciğeroğlu, E.; Özgüven, H.N. Nonlinear vibration analysis of bladed disks with dry friction dampers. *J. Sound Vib.* **2006**, *295*, 1028–1043. https://doi.org/10.1016/j.jsv.2006.02.009.
25. Stefani, G.; Angelis, M.D.; Andreaus, U. Scenarios in the experimental response of a vibro-impact SDOF system and numerical simulations. *Nonlinear Dyn.* **2020**, *100*, 3465–3488. https://doi.org/10.1007/s11071-020-05791-4.
26. Mélot, A.; Rigaud, E.; Perret-Liaudet, J. Bifurcation tracking of geared systems with parameter-dependent internal excitation. *Nonlinear Dyn.* **2022**, *107*, 413–431. https://doi.org/10.1007/s11071-021-07018-6.
27. Mélot, A. Optimizing bifurcations and singularities for performance enhancement and mitigation of the adverse dynamics of nonlinear energy sinks. *Nonlinear Dyn.* **2025**, *113*, 28635–28655. https://doi.org/10.1007/s11071-025-11638-7.
28. Mélot, A.; Rigaud, E.; Perret-Liaudet, J. Robust design of vibro-impacting geared systems with uncertain tooth profile modifications via bifurcation tracking. *Int. J. Non-Linear Mech.* **2023**, *149*, 104336. https://doi.org/10.1016/j.ijnonlinmec.2022.104336.
29. Cochelin, B.; Vergez, C. MANLAB, An Interactive Series-Expansion Approach for Continuation-Focus on Periodic Solutions. In Proceedings of the EMSC 2009, Lisbon, Portugal, 7–11 September 2009.

30. Debeurre, M.; Thomas, O. MANLAB: A Numerically-Efficient Continuation Software for the Periodic Solution of Nonlinear Systems. 2021. Available online: https://wiki.math.ntnu.no/_media/thread/start/nwt9/magic_2021_workshop_abstract_v2.pdf (accessed on 26 March 2026).
31. Slater, J.C. Mousai: An Open-Source General Purpose Harmonic Balance Solver. In Proceedings of the 13th ASME Dayton Engineering Sciences Symposium, Dayton, OH, USA, 23 October 2017. https://doi.org/10.13140/RG.2.2.33930.98245.
32. Petrov, E.P.; Ewins, D.J. Analytical formulation of friction interface elements for analysis of nonlinear multi-harmonic vibrations of bladed disks. *J. Turbomach.* **2003**, *125*, 364–371. https://doi.org/10.1115/1.1539868.
33. Petrov, E.P. A method for use of cyclic symmetry properties in analysis of nonlinear multiharmonic vibrations of bladed disks. *J. Turbomach.* **2004**, *126*, 175–183. https://doi.org/10.1115/1.1644558.
34. Petrov, E.P. Explicit finite element models of friction dampers in forced response analysis of bladed disks. *J. Eng. Gas Turbines Power* **2008**, *130*, 022502. https://doi.org/10.1115/1.2772633.
35. Petrov, E.P. A high-accuracy model reduction for analysis of nonlinear vibrations in structures with contact interfaces. *J. Eng. Gas Turbines Power* **2011**, *133*, 102503. https://doi.org/10.1115/1.4002810.
36. Lasen, M.; Salles, L.; Dini, D.; Schwingshackl, C.W. Tribomechadynamics Challenge 2021: A Multi-harmonic Balance Analysis from Imperial College London. *Conf. Proc. Soc. Exp. Mech. Ser.* **2023**, *1*, 79–82. https://doi.org/10.1007/978-3-031-04086-3_12.
37. Wagner, N.; Willerding, T. Die Methode der harmonischen Balance in der Strukturdynamik. In Proceedings of the NAFEMS Regional Conference NRC22, Bamberg, Germany, October 4–6 2022.
38. Wagner, N.; Willerding, T. The Harmonic Balance Method and its Applications in Structural Dynamics. In Proceedings of the NWC23-NAFEMS World Congress, Tampa, FL, USA, 15–18 May 2023
39. Mélot, A.; Perret-Liaudet, J.; Rigaud, E. Vibro-impact dynamics of large-scale geared systems. *Nonlinear Dyn.* **2023**, *111*, 4959–4976. https://doi.org/10.1007/S11071-022-08144-5.
40. Mahé, V.; Mélot, A.; Chouvion, B.; Droz, C. Computing the dynamic response of periodic waveguides with nonlinear boundaries using the wave finite element method. *Comput. Struct.* **2025**, *315*, 107778. https://doi.org/10.1016/j.compstruc.2025.107778.
41. Aswal, N.; Mélot, A.; Mevel, L.; Zhang, Q. Identification and monitoring of stochastic linear subsystems with unknown local nonlinearities via output injection. *Mech. Syst. Signal Process.* **2025**, *238*, 113239. https://doi.org/10.1016/j.ymssp.2025.113239.
42. Nordmark, A.B. Non-periodic motion caused by grazing incidence in an impact oscillator. *J. Sound Vib.* **1991**, *145*, 279–297. https://doi.org/10.1016/0022-460X(91)90592-8.
43. Ibrahim, R.A. *Vibro-Impact Dynamics: Modeling, Mapping and Applications*; Springer: Berlin/Heidelberg, Germany, 2009.
44. Babitsky, V.I. *Theory of Vibro-Impact Systems and Applications*; Springer: Berlin/Heidelberg, Germany, 1998.
45. Ing, J.; Pavlovskaia, E.; Wiercigroch, M.; Banerjee, S. Experimental study of impact oscillator with one-sided elastic constraint. *Philos. Trans. R. Soc. A* **2008**, *366*, 679–704. https://doi.org/10.1098/rsta.2007.2122.
46. Rebouças, G.F. Vibro-Impact Mechanics—Analytical, Numerical and Experimental Investigations. Ph.D. Thesis, Technical University of Denmark, Kgs. Lyngby, Denmark, 2018.
47. Xu, W.; Huang, D.M.; Xie, W.X. Multi-valued responses and dynamic stability of a nonlinear vibro-impact system with a unilateral offset. *Chin. Phys. B* **2016**, *25*, 030502. https://doi.org/10.1088/1674-1056/25/3/030502.
48. Liu, K.; Khulief, Y. On the harmonic responses of a vibro-impact nonlinear oscillator. *J. Sound Vib.* **2012**, *331*, 3337–3353. https://doi.org/10.1016/j.jsv.2012.04.020.
49. Bruns, P.; Twiefel, J.; Wallaschek, J. Experimental and theoretical investigation of a vibro-impact process utilizing an in situ capacitive distance measurement. In Proceedings of the ISMA 2016 Conference, Leuven, Belgium, 19–21 September 2016; ISMA 2016 Conference Paper.
50. Kharazan, M.; Irani, S.; Reza Salimi, M. Nonlinear vibration analysis of a cantilever beam with a breathing crack and bilinear behavior. *J. Vib. Control* **2022**, *28*, 2653–2665. https://doi.org/10.1177/10775463211018315.
51. Kharazan, M.; Irani, S.; Noorian, M.A.; Salimi, M.R. Nonlinear vibration analysis of a cantilever beam with multiple breathing edge cracks. *Int. J. -Non-Linear Mech.* **2021**, *136*, 103774. https://doi.org/10.1016/j.ijnonlinmec.2021.103774.
52. Wang, W.; Ma, H.; Zhao, C. Investigation of nonlinear vibrations in rotating cracked blades based on a semi-analytical method. *Mech. Based Des. Struct. Mach.* **2025**, 1–26. https://doi.org/10.1080/15397734.2025.2528162.
53. Maiti, S.; Kumar, A.; Kanchwala, H. Dynamics of a cantilever beam with solitary open crack: nonlinear response to external and base excitation. *Nonlinear Dyn.* **2025**, *113*, 7901–7936. https://doi.org/10.1007/s11071-024-10553-7.
54. Ganguly, S. Methodologies for modeling and identification of breathing crack: A review. *MethodsX* **2023**, *11*, 102420. https://doi.org/10.1016/j.mex.2023.102420.
55. Broda, D.; Mendrok, K.; Silberschmidt, V.V.; Pieczonka, L.; Staszewski, W.J. The Study of Localized Crack-Induced Effects of Nonlinear Vibro-Acoustic Modulation. *Materials* **2023**, *16*, 1653. https://doi.org/10.3390/ma16041653.
56. Long, H.; Liu, Y.; Liu, K. Nonlinear vibration analysis of a beam with a breathing crack. *Appl. Sci.* **2019**, *9*, 3874. https://doi.org/10.3390/app9183874.

57. Wu, N. Study of forced vibration response of a beam with a breathing crack using iteration method. *J. Mech. Sci. Technol.* **2015**, *29*, 2827–2835. https://doi.org/10.1007/s12206-015-0611-2.
58. El Arem, S.; Maitournam, H. A cracked beam finite element for rotating shaft dynamics and stability analysis. *J. Mech. Mater. Struct.* **2008**, *3*, 893–910.
59. Rohe, D.P.; Reu, P.L. Digital image correlation as an experimental modal analysis capability. *Exp. Tech.* **2021**, *45*, 297–312. https://doi.org/10.1007/s40799-020-00392-7.
60. Mallya, R.; Uchil, A.K.; Shenoy, S.B.; Pai, A. Application of digital image correlation in aerospace engineering: Structural health monitoring of aircraft components. *Aerosp. Syst.* **2024**, *7*, 663–680. https://doi.org/10.1007/s42401-024-00309-x.
61. Stanbridge, A.B.; Ewins, D.J. Modal testing using a scanning laser Doppler vibrometer. *Sensors* **2021**, *21*, 4705. https://doi.org/10.1006/mssp.1998.1209.
62. Mastrodicasa, D.; Lorenzo, E.D.; Manzato, S.; Peeters, B.; Guillaume, P. 3D-DIC full field experimental modal analysis of a demo airplane by using low-speed cameras and a reconstruction approach. *Mech. Syst. Signal Process.* **2025**, *222*, 111755. https://doi.org/10.1016/j.ymssp.2025.112387.
63. Scislo, L.; Drygala, I.J. 3D vibration measurements with optical systems: Selected methods for measurement enhancements. *Procedia Struct. Integr.* **2024**, *61*, 303–310. https://doi.org/10.1016/j.prostr.2024.09.352.
64. Doan, N.V.; Le, V.T.; Park, H.C.; Goo, N.S. Modal analysis using a virtual speckle pattern based digital image correlation method: An application for an artificial flapping wing. *Exp. Mech.* **2022**, *62*, 253–270. https://doi.org/10.1007/s11340-021-00775-w.
65. Andreaus, U.; Casini, P.; Vestroni, F. Nonlinear dynamics of a cracked cantilever beam under harmonic excitation. *Int. J. -Non-Linear Mech.* **2007**, *42*, 566–575. https://doi.org/10.1016/j.ijnonlinmec.2006.08.007.
66. Andreaus, U.; Baragatti, P. Fatigue crack growth, free vibrations and breathing crack detection of aluminium alloy and steel beams. *J. Strain Anal. Eng. Des.* **2009**, *44*, 595–608. https://doi.org/10.1243/03093247JSA527.
67. Andreaus, U.; Baragatti, P. Experimental damage detection of cracked beams by using nonlinear characteristics of forced response. *Mech. Syst. Signal Process.* **2012**, *31*, 382–404. https://doi.org/10.1016/j.ymssp.2012.04.007.
68. Zhao, C.; Zeng, J.; Ma, H.; Ni, K.; Wen, B. Dynamic analysis of cracked rotating blade using cracked beam element. *Results Phys.* **2020**, *19*, 103360. https://doi.org/10.1016/j.rinp.2020.103360.
69. Guan, H.; Ni, K.; Ma, H.; Xiong, Q.; Wang, W.; Wang, H. Dynamic modeling and verification of rotating compressor blade with crack based on beam element. *Appl. Math. Model.* **2024**, *133*, 618–641. https://doi.org/10.1016/j.apm.2024.05.019.
70. Al-Qaradawi, M.Y.; Balachandran, B.; Mook, D.T. Nonlinear dynamic characteristics of a simple blade with breathing crack using ANSYS software. *Sci. Res. Essays* **2011**, *6*, 1829–1842.
71. Tüfekci, M.; Sevencan, F.; Yurdakul, O. Investigating Various Nonlinear Vibration Problems Using VIBRANT: A Tool Based on Abaqus and Python. *PLoS ONE* **2026**, *21*, e0338419. https://doi.org/10.1371/journal.pone.0338419.
72. Chondros, T.G.; Dimarogonas, A.D.; Yao, J. Vibration of a beam with a breathing crack. *J. Sound Vib.* **2001**, *239*, 57–67. https://doi.org/10.1006/jsvi.2000.3156.
73. Nacivet, S.; Pierre, C.; Thouverez, F.; Jezequel, L. A dynamic Lagrangian frequency-time method for the vibration of dry-friction-damped systems. *J. Sound Vib.* **2003**, *265*, 201–219. https://doi.org/10.1016/S0022-460X(02)01447-5.
74. Vadcard, T.; Colaïtis, Y.; Batailly, A.; Thouverez, F. Assessment of Two Harmonic Balance Method-Based Numerical Strategies for Blade-Tip/Casing Interactions: Application to NASA Rotor67. In *Proceedings of the Volume 8B: Structures and Dynamics—Probabilistic Methods; Rotordynamics; Structural Mechanics and Vibration*; American Society of Mechanical Engineers: New York, NY, USA, 2022; Volume 6. https://doi.org/10.1115/GT2022-81694.